The Journal of Pharmacology and Experimental Therapeutics 393 (2026) 105004

The Journal of Pharmacology and Experimental Therapeutics

journal homepage: www.jpet.aspetjournals.org

SPECIAL SECTION: MULTISYSTEMS PHARMACOLOGY AND THERAPEUTIC APPLICATION OF ADIPOKINES AND NEUROPEPTIDES IN OBESITY—ARTICLE

# Adiponectin in cigarette smoke–induced epithelial-mesenchymal transition

Francesca Panico [1], Giuseppe Spaziano [2], Ersilia Nigro [2,3], Davida Mirra [2,*], Renata Esposito [2], Eleonora Caiazzo [2], Aurora Daniele [3,4], Bruno D'Agostino [2]

[1] *Science of Health Department, School of Medicine, University "Magna Graecia" of Catanzaro, Catanzaro, Italy*
[2] *Department of Environmental, Biological and Pharmaceutical Sciences and Technologies, University of Campania "Luigi Vanvitelli", Caserta, Italy*
[3] *CEINGE Biotecnologie Avanzate "Franco Salvatore" S.c.a r.l., Naples, Italy*
[4] *Department of Molecular Medicine and Medical Biotechnology, University of Naples Federico II, Naples, Italy*

## ARTICLE INFO

*Article history:*
Received 15 March 2026
Accepted 29 July 2026
Available online 4 August 2026

*Key words:*
Cigarette smoke
Epithelial-mesenchymal transition
Adiponectin
Oxidative stress
Normal bronchial epithelial cells
Lung adenocarcinoma epithelial cells

## ABSTRACT

Cigarette smoke (CS) contributes to a wide range of chronic respiratory diseases by inducing epithelial-mesenchymal transition (EMT), which drives tissue remodeling, fibrosis, and tumor progression. In this scenario, adiponectin (Acrp30) has emerged as a potential EMT-negative regulator, inhibiting migration and invasion in non–small cell lung cancer cell lines. This study aimed to investigate ability of Acrp30 to prevent CS-induced EMT and profibrotic remodeling in normal and adenocarcinoma lung cells, through AdipoRon, a synthetic Acrp30 receptor agonist. BEAS-2B and A549 cells were used to preliminarily assess the optimal dose and timing for CS and AdipoRon exposure for subsequent evaluations by thiazolyl blue tetrazolium bromide assay. Expression of epithelial (E-cadherin), mesenchymal (vimentin), and profibrotic ($\alpha$-smooth muscle actin, transforming growth factor-$\beta$, total collagen deposition, and collagen type I $\alpha$1 chain) markers was examined through immunofluorescence, reverse transcription polymerase chain reaction, and Sirius Red staining. Wound-healing assay was used to assess CS and Acrp30 ability to influence cell migration. Reactive oxygen species levels were measured by 2′,7′-dichlorofluorescin diacetate assay. Acrp30 prevents CS-induced dysregulation of E-cadherin and vimentin at both mRNA and protein levels, preserving the epithelial-mesenchymal balance in both cell lines. Furthermore, CS-induced increase in profibrotic marker expression was significantly attenuated by AdipoRon pretreatment in both BEAS-2B and A549 cells. The CS-induced increase in migratory capacity was significantly reversed by Acrp30 in both cell lines, confirming its ability to prevent EMT. Finally, Acrp30 also markedly reduced CS-induced reactive oxygen species overproduction in BEAS-2B and A549 cells, indicating a role in modulating oxidative stress-driven epithelial plasticity. Thus, Acrp30 effectively preserves epithelial markers, limits the mesenchymal shift and profibrotic remodeling, and reduces migratory capacity by mitigating oxidative stress. These results support Acrp30 as a promising therapeutic candidate for preventing airway remodeling and disease progression in smoking-related conditions.

*Significance Statement:* Cigarette smoke (CS) induces epithelial-mesenchymal transition and fibrosis in both healthy and cancerous lung epithelial cells. Adiponectin pretreatment prevents CS-induced epithelial-mesenchymal transition and profibrotic remodeling in both cell lines; adiponectin can prevent airway remodeling and disease progression in CS conditions.



* **Address correspondence to:** Dr Davida Mirra, Department of Environmental, Biological and Pharmaceutical Sciences and Technologies, University of Campania "Luigi Vanvitelli", Caserta, Italy. E-mail: davida.mirra@unicampania.it

This article has supplemental material available at jpet.aspetjournals.org.

F.P. and G.S. contibuted equally to this work.

https://doi.org/10.1016/j.jpet.2026.105004

## 1. Introduction

### 1.1. Cigarette smoke–induced lung injury and epithelial-mesenchymal transition

Cigarette smoke (CS) is a mixture of many different chemical compounds and represents a widely recognized primary risk factor for several lung conditions, including chronic obstructive pulmonary disease (COPD) and lung cancer.[1–3] CS exposure can lead to chronic pulmonary injury and dysfunction through different complex mechanisms, including DNA damage, epigenetic alternation, oxidative stress, and alteration in inflammatory pathways.[4–11] The bronchial and alveolar epithelium are the first line of defense against inhaled toxicants such as those contained in CS,[12–16] which can lead to significant alterations of epithelial integrity and cell function, ultimately promoting epithelial-mesenchymal transition (EMT), a crucial event in tissue remodeling, tumor progression, and metastasis.[17–20] At the molecular level, the EMT process is defined by the downregulation of epithelial junction proteins such as E-cadherin as well as the upregulation of mesenchymal markers such as vimentin.[21] EMT not only contributes to tissue remodeling and fibrosis but is also involved in carcinogenesis and metastasis.[22,23] Indeed, in lung cancer, EMT drives the invasion process through desmoplastic stroma formation and contributes to the conversion of cancer cells into invasive malignant phenotypes.[24,25] Additionally, in the small airway of smokers with COPD who develop lung cancer, EMT plays a key role in airway remodeling and cancer progression.[26]

### 1.2. Oxidative stress as a driver of CS-induced EMT

Oxidative stress is a critical driver of EMT induction. Although the exact signaling pathways through which reactive oxygen species (ROS) promote this process remain unclear, ROS can modulate cellular signaling to activate EMT-associated pathways and drive the acquisition of a cancerous phenotype.[27] CS, in addition to direct oxidative injury, promotes the trafficking and persistence of inflammatory cells in the lung. These immune cells, particularly neutrophils and macrophages, release a range of chemotactic and cytotoxic mediators, such as proteolytic enzymes and ROS, contributing to extracellular matrix degradation and epithelial barrier dysfunction.[28–30] Currently, bronchodilators and anti-inflammatory agents, commonly drugs used for the treatment of smoke-related lung injury,[31] are not able to act on EMT, highlighting the urgent need to identify new therapeutic targets.

### 1.3. Adiponectin as a potential regulator of epithelial plasticity and tumor progression

Adiponectin (Acrp30), an adipokine produced by adipose tissues and well established as a pleiotropic mediator,[32] plays a critical role in the lung microenvironment by reducing local inflammation and inhibiting alveolar macrophage activation.[33] This adipokine exerts its biological functions through specific receptors, adiponectin receptor 1 (AdipoR1), AdipoR2, and T-cadherin. Dysregulation of the Acrp30 system has been reported in several malignancies, including non–small cell lung carcinoma (NSCLC). Previously, we observed reduced levels of total adiponectin and T-cadherin as well as an increase in high molecular weight oligomers and AdipoR1 in NSCLC lung tissue, suggesting a dysfunctional Acrp30 axis.[34] Emerging evidence indicates that Acrp30 may inhibit migration and invasion by suppressing the EMT process in NSCLC cells.[35] However, the study by Cui et al[35] focused on Acrp30 effects in established NSCLC cells under basal conditions, without addressing the contribution of CS, which is the major etiological factor in lung carcinogenesis and a key inducer of EMT-related alterations in airway epithelium. In patients with nasopharyngeal carcinoma, an inverse correlation has been observed between serum Acrp30 level and tumor stage, recurrence and metastasis, and poor metastasis-free survival.[36] Furthermore, circulating Acrp30 levels are reduced in smokers, suggesting a potential link between Acrp30 deficiency and increased susceptibility to smoke-induced lung conditions.[37]

### 1.4. Study aim

The potential of Acrp30 in counteracting CS-induced EMT onset in healthy epithelium as well as in tumor progression has not been fully elucidated. Therefore, the aim of this study was to investigate the protective effects of Acrp30 against CS-induced EMT, to our knowledge, here addressed for the first time, in healthy and cancerous lung epithelial cells, through AdipoRon, a synthetic Acrp30 agonist that activates the AMP-activated protein kinase and peroxisome proliferator-activated receptor-$\alpha$ pathways, reducing oxidative stress and inflammation.[38]

## 2. Materials and methods

### 2.1. Cell culture and treatment

The normal human bronchial epithelial cell line BEAS-2B was purchased from American Type Culture Collection (ATCC CCL-185) and cultured in RPMI-1640 Medium (Gibco) supplemented with 10% FBS (Gibco) and 1% penicillin/streptomycin (Gibco) at 37 °C and in 5% $CO_2$/95% humidified air. The human lung adenocarcinoma cell line A549 was purchased from ATCC (ATCC CCL-185) and cultured in Dulbecco's modified Eagle's medium/nutrient mixture F-12 (Gibco) supplemented with 10% FBS (Gibco) and 1% penicillin/streptomycin (Gibco) at 37 °C and in 5% $CO_2$/95% humidified air. Both cell lines were grown in 75 $cm^2$ tissue culture flasks. Confluence was reached after 3 to 4 days in culture, and all experiments were performed on cells between passage 15 and 25. The AdipoRon compound (Merck) was solubilized in DMSO to produce a stock solution (Sigma-Aldrich) and subsequently diluted to working concentration. Three independent experiments for each evaluation were performed in both cell lines.

### 2.2. Preparation of CS extract

The cigarette smoke extract (CSE) was prepared by bubbling 10 Red Marlboro cigarettes (Phillip Morris), as previously reported.[39] The obtained extract was considered as 100% CSE. The CSE was sterile-filtered through a 0.20-$\mu$m pore filter, aliquoted, and stored at −80 °C to reduce variability and ensure reproducibility across all experiments. Before use, CSE was diluted with RMPI or Dulbecco's modified Eagle's medium to the indicated concentration.

### 2.3. Thiazolyl blue tetrazolium bromide assay

BEAS-2B or A549 cells were used to determine the timing and optimal dose for CSE and AdipoRon exposure for subsequent analyses. The cells were seeded at a density of $1 \times 10^4$ per well in 96-well plates and allowed to attach overnight at 37 °C in 5% $CO_2$/95% humidified air. The cells were then exposed to increasing CSE concentrations, ranging from 1% to 20% for 24 hours. In another set of experiments, cells were exposed to increasing AdipoRon concentrations ranging from 5 to 50 $\mu$g/mL for 24 and 48 hours. Cellular viability was determined by the thiazolyl blue tetrazolium bromide assay (M5655, Sigma-Aldrich). Briefly, 25 $\mu$L of thiazolyl blue tetrazolium bromide (2 mg/mL) was added to each well and

incubated for 4 hours to perform the proliferation assay. After this time, DMSO was added to measure the absorbance. The cellular viability was calculated as the percentage of absorbance at 570 nm of untreated cells using a microplate reader (GloMax Explorer, Promega).

### 2.4. ROS determination

To evaluate the AdipoRon potential to counteract CSE effects on the redox balance of BEAS-2B or A549 cells, ROS species were measured with 2′,7′-dichlorodihydrofluorescein diacetate assay. The cells were seeded at a density of $1 \times 10^4$ per well in 96-well plates and allowed to attach overnight at 37 °C in 5% $CO_2$/95% humidified air. The cells were then pretreated or not for 2 hours with AdipoRon (10 $\mu$g/mL) or 1 mM N-acetylcysteine (NAC), used as an antioxidant control, and then exposed to 2% or 10% CSE for 24 hours. $H_2O_2$ was used as a positive oxidative stress control in the presence or absence of NAC. After treatments, 200 $\mu$L of 50 $\mu$M 2′,7′-dichlorodihydrofluorescein diacetate (Merck) in Hanks' balanced salt solution (Sigma-Aldrich) were added in each well and incubated for 1 hour at 37 °C. Then, the cells were subsequently washed 3 times with PBS to remove the extracellular fluorescent compounds and minimize background signal. Fluorescence was measured at an excitation wavelength of 540 nm and an emission wavelength of 590 nm using a microplate reader (GloMax Explorer, Promega). The relative ROS production was normalized to the fluorescence intensity of untreated control cells.

### 2.5. Reverse transcriptase and quantitative real-time polymerase chain reaction

mRNA basal expression levels of AdipoR1 and AdipoR2 were preliminarily evaluated in both cell lines. Moreover, to evaluate the ability of AdipoRon to counteract CSE effects on fibrosis and EMT, the expression of transforming growth factor-$\beta$ (TGF-$\beta$), epithelial (E-cadherin), and mesenchymal (vimentin) markers was examined through reverse transcription polymerase chain reaction (RT-PCR). Notably, $1 \times 10^6$ cells per well BEAS-2B and A549 were seeded in 6-well plates and allowed to attach overnight at 37 °C in 5% $CO_2$/95% humidified air. Both cell lines were pretreated or not for 2 hours with AdipoRon (AR) and then exposed to 2% or 10% CSE for 24 hours. Cells were then lysed and total RNA was extracted using the TRIzol method. Then, 2 $\mu$g of total RNA was subjected to RT-PCR using the High-Capacity cDNA Reverse Transcription Kit (Thermo Fisher Scientific), according to the manufacturer's instructions. The thermocycling conditions were set as follows: 25 °C for 10 minutes, 37 °C for 120 minutes, 85 °C for 5 minutes, and 4 °C hold. RT-PCR was performed using the TaqMan Universal PCR Master Mix (Thermo Fisher Scientific) according to the manufacturer's instructions and QuantumStudio3 Real-Time PCR Systems. The thermocycling conditions were set as follows: 50 °C for 2 minutes, 95 °C for 10 minutes, 95 °C for 15 seconds, and 60 °C for 1 minutes. Data from all RT-PCR experiments and mRNA expression levels were normalized to the endogenous housekeeping gene control applying the comparative $2^{-\Delta\Delta Ct}$ method, where $\Delta Ct = Ct_{mRNA} - Ct_{housekeeping\ mRNA}$, whereas the relative quantification of differences in expression was conducted with $\Delta\Delta Ct = \Delta Ct_{TREATMENT} - \Delta Ct_{CTR}$.

### 2.6. Immunofluorescence staining

To further investigate AdipoRon's ability to prevent CSE effects on EMT and profibrotic remodeling, expression of E-cadherin, vimentin, $\alpha$-smooth muscle actin ($\alpha$-SMA), and collagen type I $\alpha$1 chain (COL1A1) was evaluated through immunofluorescence staining. BEAS-2B and A549 cells were seeded on 12-mm coverslips at a density of $5 \times 10^4$ per well in 24-well plates and allowed to attach overnight at 37 °C in 5% $CO_2$/95% humidified air. Both cell lines were pretreated or not for 2 hours with AdipoRon and then exposed to 2% or 10% CSE for 24 hours. After treatments, cells were washed 3 times in PBS, fixed in 4% formaldehyde at room temperature for 20 minutes, followed by permeabilization with 1% Triton X-100 in PBS for 10 minutes. Cells were then washed 3 times with PBS and stained with an antivimentin /E-cadherin/COL1A1 (ABclonal; Elabscience) and anti-$\alpha$-SMA (Sigma-Aldrich) antibodies followed by donkey anti-rabbit IgG 555/488 (Alexa Fluor) and donkey anti-mouse IgG 555 (Alexa Fluor) secondary antibodies. After staining, the coverslips were rinsed in PBS and mounted on glass slides. Images were acquired with an Apotome.2 microscope (Zeiss) at 20× magnification and analyzed with ImageJ software (National Institutes of Health, NIH).

### 2.7. Sirius Red staining

Total collagen deposition was assessed in BEAS-2B and A549 cells by Sirius Red staining. Cells were seeded at a density of $1 \times 10^4$ per well in 96-well plates and allowed to attach overnight at 37 °C in 5% $CO_2$/95% humidified air. Both cell lines were pretreated or not for 2 hours with AdipoRon and then exposed to 2% or 10% CSE for 24 hours. After treatments, cells were washed once with PBS and then fixed with 4% formaldehyde for 20 minutes at room temperature. Following fixation, cells were washed 3 times with PBS and incubated with 50 $\mu$L of 0.1% Sirius Red (Direct Red 80; Sigma-Aldrich) prepared in 1% acetic acid for 60 minutes at room temperature. Cells were then washed with 0.1 M HCl and then 0.1 M sodium hydroxide (NaOH) solution was added to each well to eluate the bound dye from the cell-associated collagens. Representative images of stained wells were acquired before dye elution. Subsequently, 100 $\mu$L of the eluted solution was transferred to a new 96-well plate, and absorbance was measured at 540 nm using a microplate reader (GloMax Explorer, Promega). The relative collagen content was normalized to the absorbance of untreated control cells.

### 2.8. Wound-healing assay

To further explore AdipoRon's potential in counteracting CSE-induced EMT, cell migration was examined through the wound-healing assay. BEAS-2B and A549 cells were seeded at a density of $2 \times 10^5$ cells/well into a 12-well plate and allowed to attach overnight at 37 °C in 5% $CO_2$/95% humidified air. The monolayer was scratched using a sterile tip and washed with PBS to remove detached cells. Then the cells were pretreated or not for 2 hours with AdipoRon and then exposed to 2% or 10% CSE for 24 hours. Both cell lines were photographed at 4, 12, and 24 hours post-wounding. The relative closure area of the wound at the chosen time points was normalized to the initial wound area of untreated cells.

### 2.9. Statistical analysis

The normal distribution of data was assessed before statistical analysis using appropriate tests. Specifically, normal distribution was evaluated using the Shapiro-Wilk test. Variables showing normal distribution were analyzed with parametric tests. The one-way ANOVA followed by Tukey multiple comparison test were used for statistical analyses using the GraphPad software (version 9.0) (GraphPad Software). Differences were considered statistically significant at $P < .05$. Data are presented as the mean ± SD.

Only statistically significant differences relevant to the purpose of this study are displayed in the graphs.

## 3. Results

### 3.1. CS effects on cellular viability

To determine the optimal CSE exposure for downstream analyses, BEAS-2B and A549 cells were treated with different concentrations of CSE for 24 hours. Both cell lines showed a dose-dependent decrease in viability, with the most pronounced reduction observed at 5% CSE for BEAS-2B ($P < .0001$) and 10% CSE for A549 ($P < .0001$) (Fig. 1, A and C). From these concentrations onward, no further decrease was observed in either cell line. In BEAS-2B, evident morphological alteration, including cell rounding and partial detachment, became significant starting from 5% CSE (Fig. 1B), whereas significant morphological changes in A549 cells were evident only upon exposure to the highest concentration of CSE (Fig. 1D). Based on these results, 2% CSE for BEAS-2B and 10% CSE for A549 were selected as working concentrations for subsequent experiments, representing the doses at which the most pronounced functional impairments were observed, without altering cell morphology.

### 3.2. AR effects on cellular viability

To establish the exact dose and exposure time of AR for downstream analyses, BEAS-2B and A549 cells were treated with increasing concentrations of AR ranging from 5 to 50 $\mu$g/mL for 24 or 48 hours (Fig. 2). After 24 hours, BEAS-2B viability was unaffected at 5 and 10 $\mu$g/mL, whereas 50 $\mu$g/mL induced a significant ~40% reduction ($P < .01$) (Fig. 2A). After 48 hours, BEAS-2B cells exhibited a reduction in viability across both AR-treated and corresponding vehicle-treated groups, with the most pronounced effect observed at 50 $\mu$g/mL ($P < .0001$) (Fig. 2B). In contrast, A549 cells did not show significant changes in viability at any AR concentration or time point (Fig. 2, C and D). Based on these findings, 10 $\mu$g/mL AR was selected as the optimal and noncytotoxic working condition for both cell lines, whereas the 2-hour pretreatment was established in accordance with previous reports[40–42] for subsequent experiments.

### 3.3. AR pretreatment modulation of CSE-induced EMT markers dysregulation

Basal expression levels of AdipoR1 and AdipoR2 were preliminarily evaluated in both cell lines. BEAS-2B cells showed

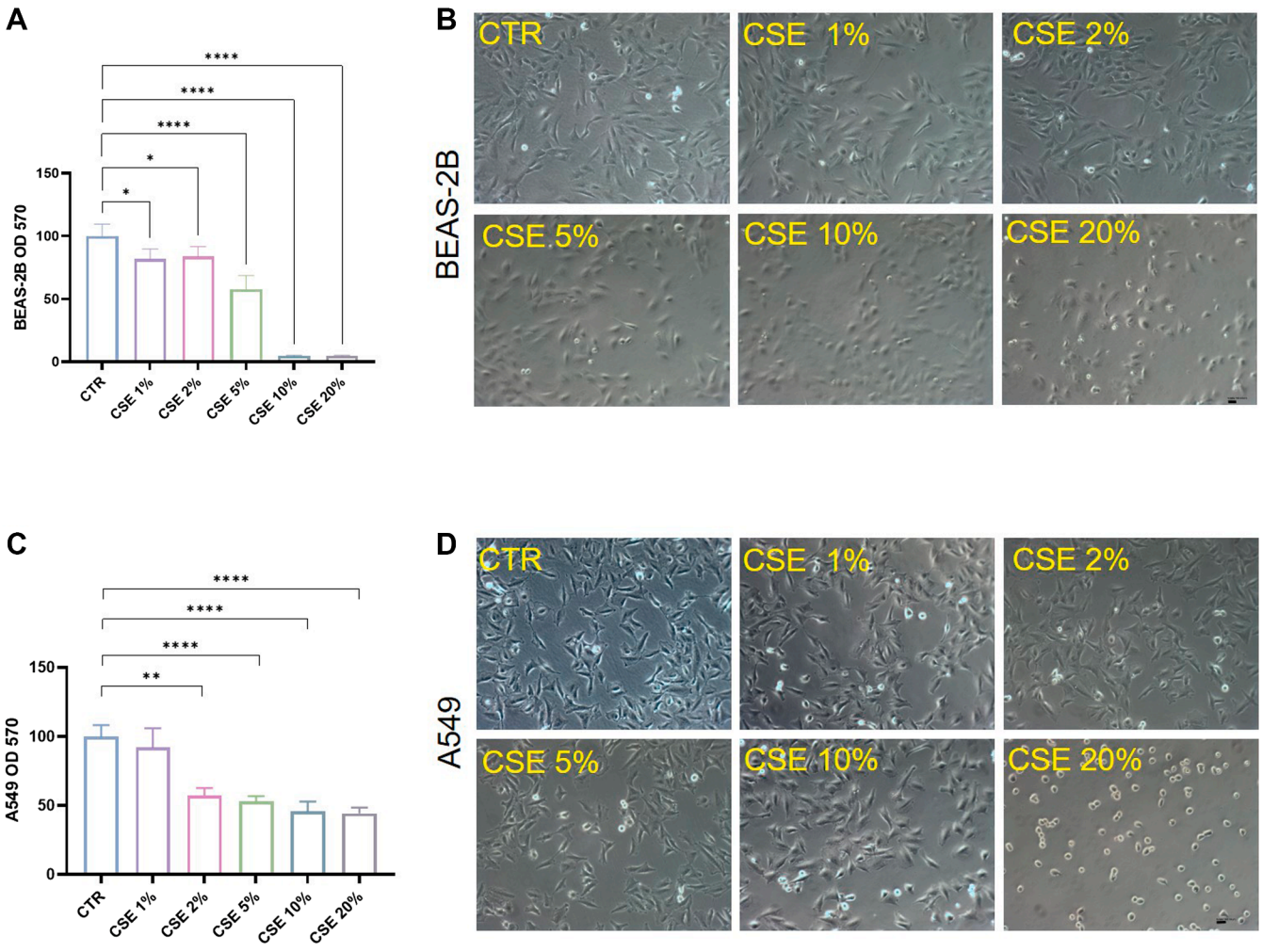


**Fig. 1.** BEAS-2B and A549 cells were used to assess the exact dose of CSE exposure for downstream analyses. Both cell lines were exposed to different CSE concentrations ranging from 1% to 20% for 24 hours. Following treatments, cellular viability was determined by the thiazolyl blue tetrazolium bromide assay. The relative cellular viability was calculated as the percentage of absorbance at 570 nm of untreated cells (A and B). Representative images of BEAS-2B (C) and A549 (D) cells treated with increasing concentrations of CSE. Scale bar, 100 $\mu$m. Data are representative of 3 independent experiments, and values are expressed as mean ± SD. The statistical test used in these analyses was one-way ANOVA followed by Tukey multiple comparison test. *$P < .05$, **$P < .01$, ****$P < .0001$.

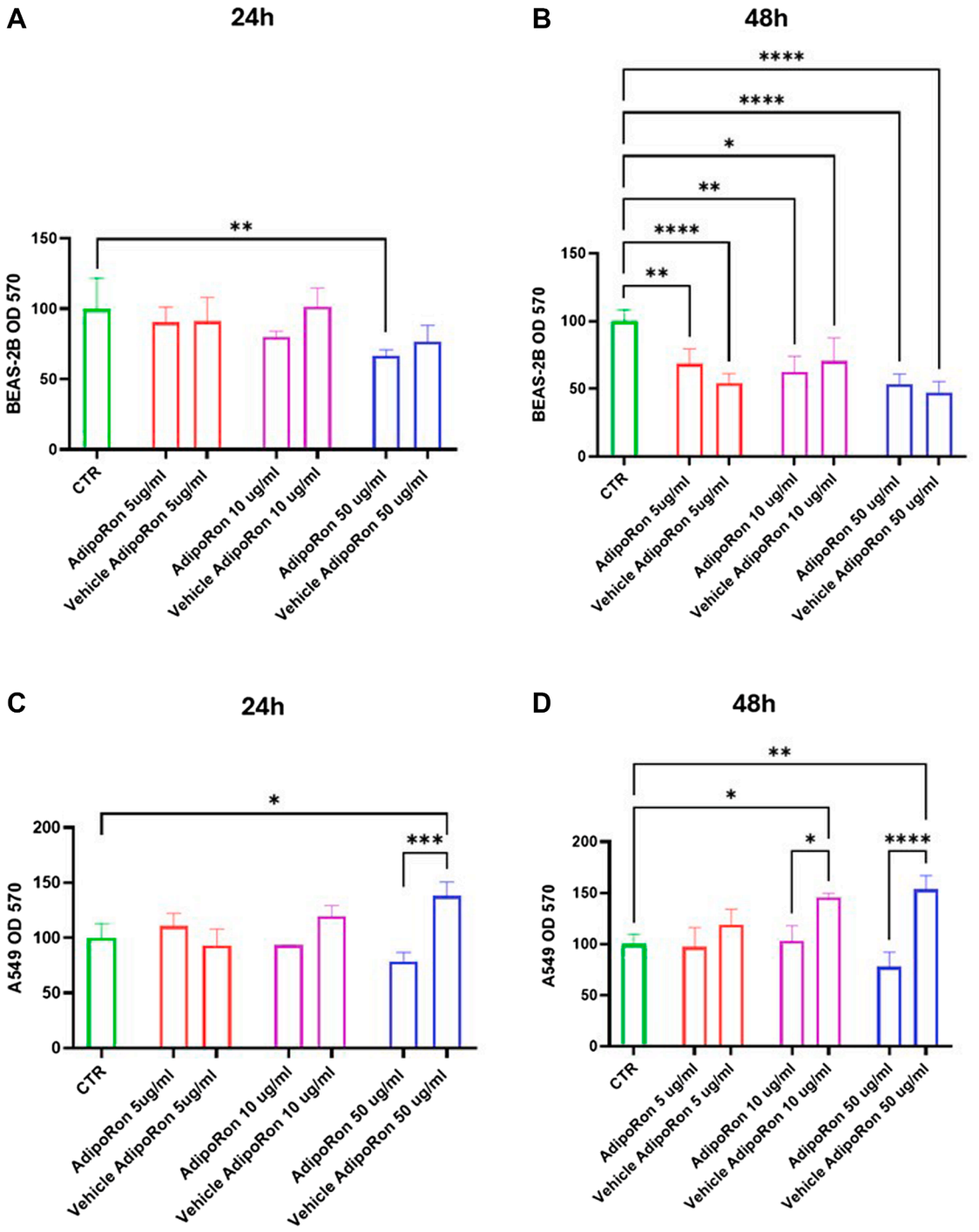


**Fig. 2.** BEAS-2B and A549 cells were used to assess the exact dose and timing of AR exposure for downstream analyses. Both cell lines were exposed to different AR concentrations ranging from 5 to 50 $\mu$g/mL for 24 hours (A and C) and 48 hours (B and D). Following treatments, cellular viability was determined by the thiazolyl blue tetrazolium bromide assay. The relative cellular viability was calculated as the percentage of absorbance at 570 nm of untreated cells. Data are representative of 3 independent experiments, and values are expressed as mean ± SD. The statistical test used in these analyses was one-way ANOVA followed by Tukey multiple comparison test. *$P < .05$, **$P < .01$, ***$P < .001$, ****$P < .0001$.

significantly higher expression of both receptors compared with A549 cells ($P < .0001$) (Supplemental Fig. 1). To assess the potential AR ability to counteract CSE-induced EMT, the mRNA expression levels of mesenchymal (vimentin) and epithelial (E-cadherin) markers were analyzed by RT-PCR in both cell lines. CSE exposure led to a marked upregulation of vimentin ($P < .05$ in both cell lines) (Fig. 3, A and C) and a concomitant downregulation of E-cadherin ($P < .05$ in BEAS-2B and $P < .001$ in A549) (Fig. 3, B and D) mRNA expression levels compared with the control (CTR) group. Although AR alone did not significantly affect the mRNA expression levels of vimentin and E-cadherin, AR pretreatment significantly prevented CSE effects on vimentin and E-cadherin levels ($P < .01$ and $P < .05$ in both cell lines, respectively) by restoring the expression of these markers toward CTR levels (Fig. 3). To further validate these findings, the expression of the above-mentioned markers was detected also by immunofluorescence staining (Fig. 4, A and C; Fig. 5, A and C). Consistent with the RT-PCR results, CSE increased vimentin levels ($P < .01$ in BEAS-2B; $P < .05$ in A549)

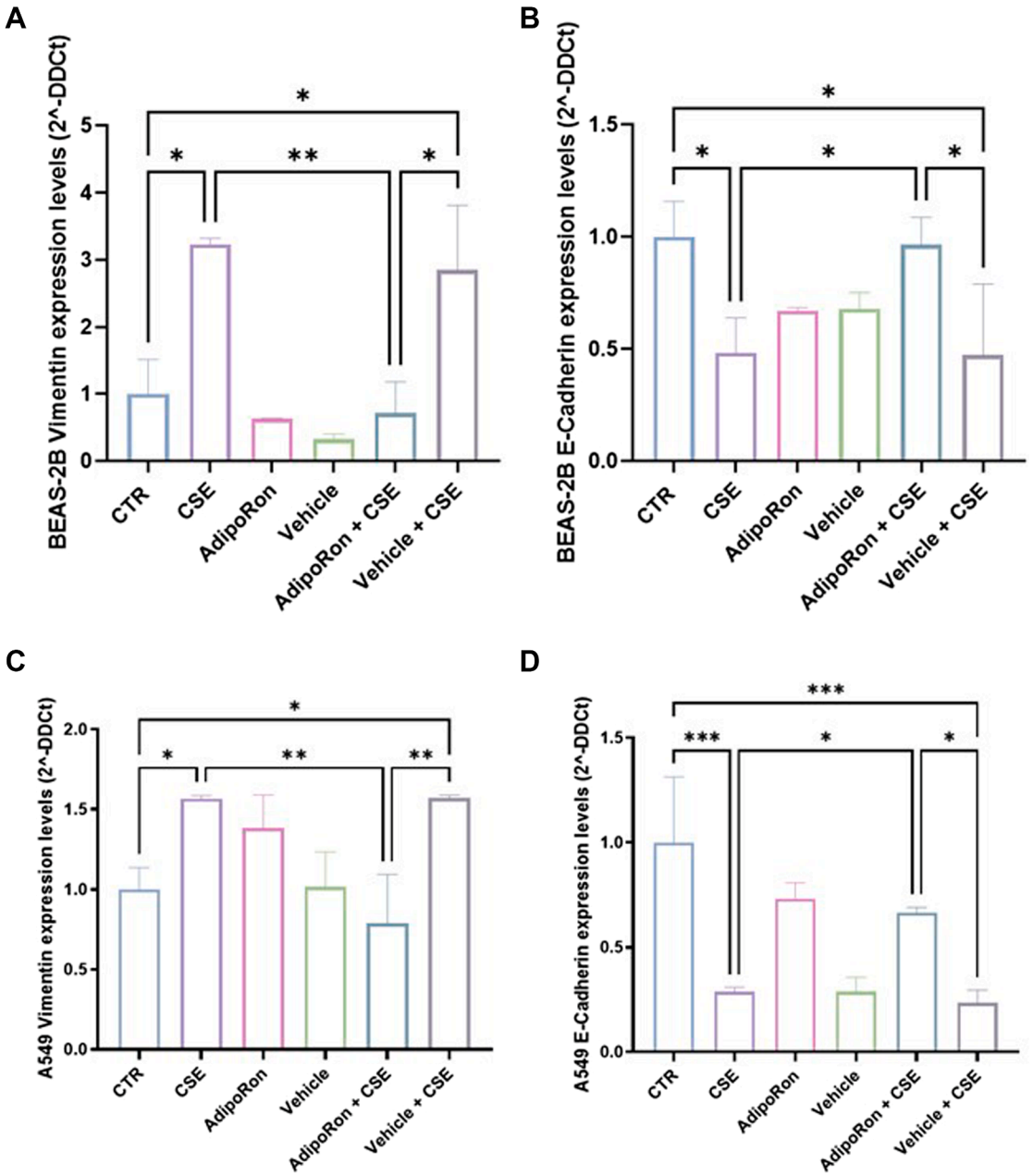


**Fig. 3.** RT-PCR analysis of EMT marker expression in BEAS-2B and A549 cells. The mRNA expression levels of the mesenchymal marker vimentin (A and C) and the epithelial marker E-cadherin (B and D) were evaluated to assess AR ability to mitigate CSE effects on EMT. Cells were pretreated or not for 2 hours with AR and then exposed to CSE for 24 hours before performing RT-PCR. Data from all RT-PCR experiments and mRNA expression levels were analyzed by normalizing to the endogenous housekeeping gene control applying the comparative $2^{-\Delta\Delta Ct}$ method. Data are representative of 3 independent experiments, and values are expressed as mean ± SD. The statistical test used in these analyses was one-way ANOVA followed by Tukey multiple comparison test. *$P < .05$, **$P < .01$, ***$P < .001$.

(Fig. 4A; Fig. 5A) and markedly reduced E-cadherin ($P < .001$ in BEAS-2B; $P < .0001$ in A549) (Fig. 4C; Fig. 5C) at the protein level. AR pretreatment mitigated these changes, preserving the epithelial ($P < .05$ in both cell lines) and mesenchymal ($P < .01$ in BEAS-2B; $P < .05$ in A549) balance. Fluorescence imaging showed that CSE ability to promote the transition of epithelial cells toward a mesenchymal phenotype and AR protective role in preventing these alterations (Fig. 4, B and D; Fig. 5, B and D).

### 3.4. Role of AR in CSE-induced profibrotic response

To investigate AR and CSE effects on profibrotic pathways, the expression of the profibrotic mediators $\alpha$-SMA and TGF-$\beta$, total collagen deposition, and collagen type I protein was evaluated in both cell lines. As shown in Fig. 6, A and C, $\alpha$-SMA expression was markedly enhanced following CSE exposure in both cell lines ($P <$ .01 vs CTR). This response was significantly blunted by AR pretreatment, which reduced $\alpha$-SMA levels in BEAS-2B and A549 cells ($P < .0001$ and $P < .05$, respectively) (Fig. 6, A and C). Figure 6, B and D show representative immunofluorescence images of labeled $\alpha$-SMA. RT-PCR analysis revealed a significant increase in TGF-$\beta$ mRNA expression following CSE exposure compared with CTR cells ($P < .001$ in both cell lines) (Fig. 6, E and F), indicating the activation of signaling pathways involved in both EMT progression and early fibrotic remodeling. AR pretreatment significantly attenuated this response ($P < .001$ in A549 and $P < .01$ in BEAS-2B),

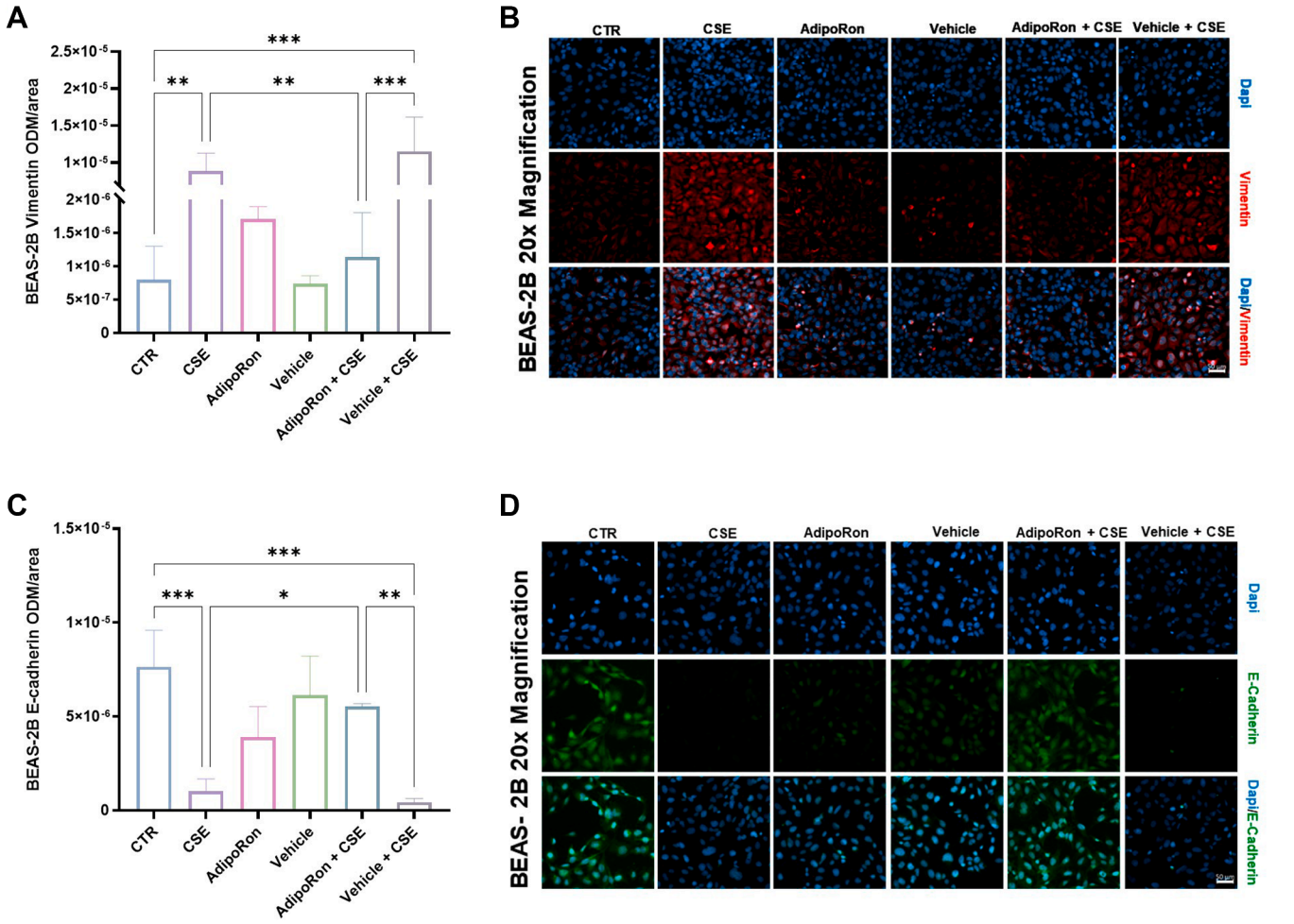


**Fig. 4.** Immunofluorescence staining of EMT marker expression in BEAS-2B. The expression of the mesenchymal marker vimentin (A) and the epithelial marker E-cadherin (C) was evaluated to assess AR ability to mitigate CSE effects on EMT. Cells were pretreated or not for 2 hours with AR and then exposed to CSE for 24 hours before performing immunofluorescence staining. Data are representative of 3 independent experiments, and values are expressed as mean ± SD. The statistical test used in these analyses was one-way ANOVA followed by Tukey multiple comparison test. *$P < .05$, **$P < .01$, ***$P < .001$. Representative images of labeled vimentin (B) and E-cadherin (D) proteins in BEAS-2B cells. Scale bar, 50 $\mu$m. Cell fluorescence images were acquired by the Apotome.2 microscope (Zeiss) and analyzed with ImageJ software (NIH).

restoring TGF-$\beta$ expression toward CTR levels (Fig. 6, E and F). Collagen deposition was then quantified by Sirius Red staining. CSE exposure significantly increased total collagen content compared with untreated cells ($P < .05$ in BEAS-2B and $P < .001$ in A549), while AR pretreatment markedly reduced collagen accumulation ($P < .0001$ in both cell lines) (Fig. 7, A and C), reflecting its ability to attenuate the CSE-induced profibrotic effect. Representative Sirius Red images show collagen content in both cell lines, indicating more intense staining in CSE-treated cells and a substantial reduction following AR exposure (Fig. 6, B and D). COL1A1 protein levels, assessed by immunofluorescence staining, followed a similar trend. Notably, CSE exposure significantly enhanced COL1A1 expression compared with CTR cells ($P < .0001$ in A549 and $P < .01$ in BEAS-2B), whereas AR pretreatment significantly prevented this increase ($P < .001$ in both cell lines) (Fig. 7, E and G). Fluorescence images show these findings, in Fig. 7, F and H.

### 3.5. AR pretreatment effects on CSE-induced enhancement of cell migratory capacity

BEAS-2B and A549 migration and the wound closure phenomenon were monitored at 4, 12, and 24 hours postscratch. The relative closure area of the wound at the chosen time points was normalized to the initial wound area of untreated cells, as shown in Fig. 8, A and B. No statistically significant differences were observed in cell migration between experimental groups at 4 (Fig. 8A) and 12 hours (data not shown) for both cell lines. However, at 24 hours, BEAS-2B (Fig. 8A) and A549 (Fig. 8B) cells exposed to CSE showed a significantly reduced scratch area compared with the CTR group ($P < .001$ and $P < .05$, respectively). In contrast, pretreatment with AR led to a significantly residual wound area at 24 hours in both cell lines ($P < .0001$, respectively), reflecting a reduction in cell migratory potential and a slower wound healing process. Figure 8, C and D display the scratch-wound closure over time, highlighting the temporal progression of wound healing. Figure 8, E and F display representative micrographs of scratch areas at 4 and 24 hours.

### 3.6. AR pretreatment impact on CSE-induced oxidative unbalance

To evaluate whether AR and CSE effects on redox status, intracellular ROS levels were measured in BEAS-2B and A549 cells. CSE exposure markedly increased ROS production ($P < .05$ in BEAS-2B and $P < .001$ for A549) (Fig. 9), compared with untreated controls, confirming its ability to induce oxidative stress. Pretreatment with AR significantly attenuated these effects, demonstrating ROS-

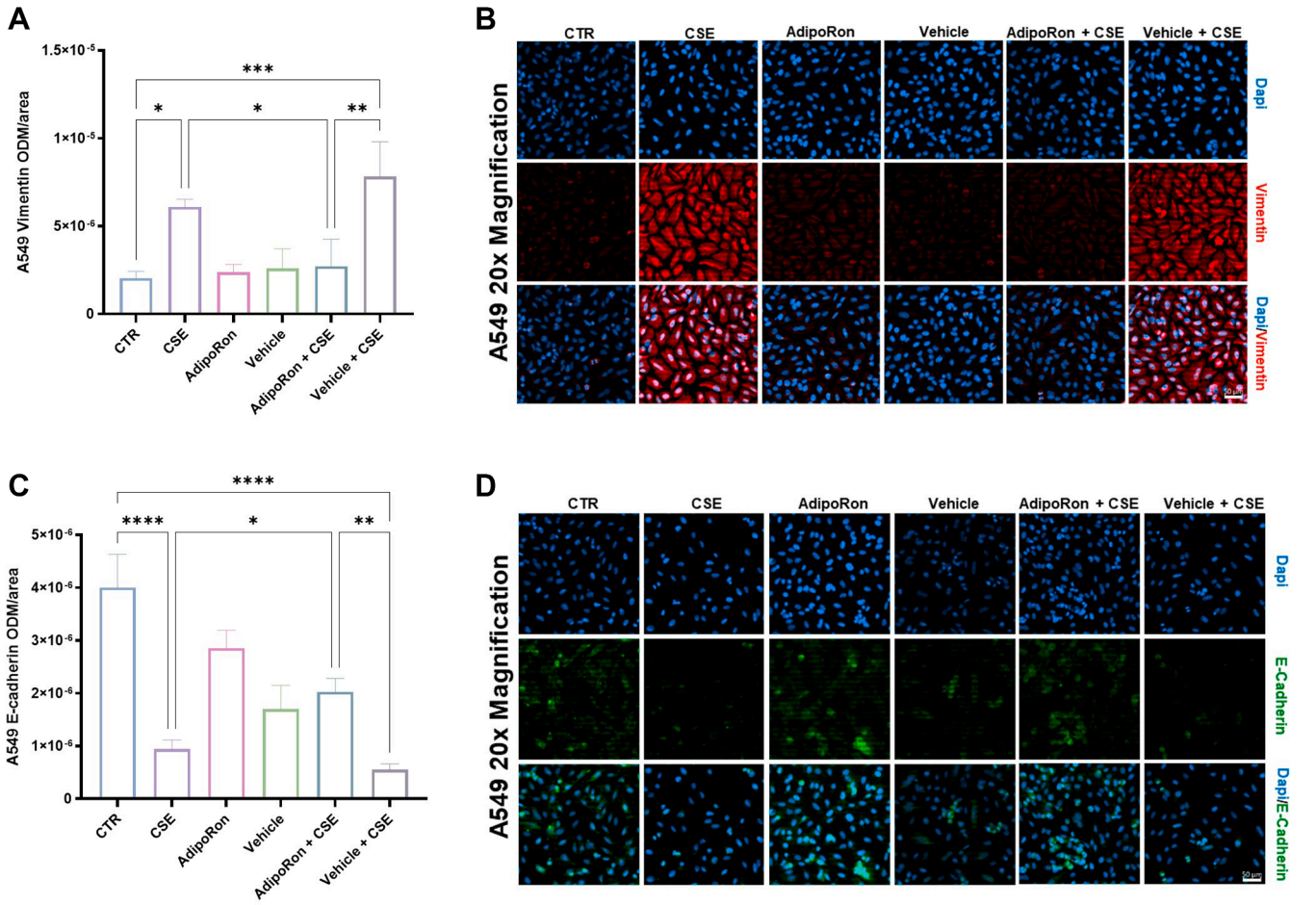


**Fig. 5.** Immunofluorescence staining of EMT marker expression in A549 cells. The expression of the mesenchymal marker vimentin (A) and the epithelial marker E-cadherin (B) was evaluated to assess AR ability to mitigate CSE effects on EMT. Cells were pretreated or not for 2 hours with AR and then exposed to CSE for 24 hours before performing immunofluorescence staining. Data are representative of 3 independent experiments, and values are expressed as mean ± SD. The statistical test used in these analyses was one-way ANOVA followed by Tukey multiple comparison test. *$P < .05$, **$P < .01$, ***$P < .001$, ****$P < .0001$. Representative images of labeled vimentin (B) and E-cadherin (D) proteins in A549 cells. Scale bar, 50 $\mu$m. Cell fluorescence images were acquired by the Apotome.2 microscope (Zeiss) and analyzed with ImageJ software (NIH).

scavenging activity by restoring redox balance in BEAS-2B ($P < .0001$) (Fig. 9A) and A549 cells ($P < .05$) (Fig. 9B). Similarly, treatment with the antioxidant control NAC significantly attenuated CSE-induced ROS generation ($P < .0001$ for both cell lines) (Fig. 9) and effectively counteracted $H_2O_2$-induced oxidative stress in BEAS-2B ($P < .0001$) and A549 ($P < .05$) (Fig. 9). Overall, these findings support the antioxidant activity of AR against CSE-induced oxidative imbalance.

## 4. Discussion

### 4.1. Acrp30 counteracts CS-induced EMT and fibrotic remodeling

This study highlights the role of Acrp30 as a negative modulator of EMT and profibrotic response driven by CS, restoring epithelial marker expression and reducing migratory capacity. A growing body of evidence indicates that CS-induced pathological remodeling of the respiratory epithelium is largely driven by EMT, a dynamic process implicated in airway structural changes and tumor progression.[17–20] In this context, Acrp30 has been identified as a negative modulator of EMT.[35] Moreover, reduced systemic Acrp30 levels have been observed in current smokers compared with never smokers.[37] However, its role in counteracting CS-induced EMT in both normal and malignant lung epithelial cells remains poorly understood. Exposure to CSE significantly reduced the viability of both healthy bronchial epithelial cells and lung adenocarcinoma cell models, accompanied by morphological alterations such as cell rounding and detachment, indicative of cellular stress. Consistent with our findings, different studies reported a similar CSE cytotoxicity of pulmonary cells confirming its ability to compromise epithelial cell integrity.[18,43,44] EMT has been reported as an active process in CS-associated COPD, where reticular basement membrane hypervascularity and fibrotic remodeling are closely related to ongoing EMT in pulmonary lesions.[45] CS-induced EMT leads to endothelial cells and epithelial barrier dysfunction, interferes with tissue repair, ultimately leading to airway fibrosis.[31] In accordance with these evidence, in our study, normal bronchial epithelial cells exposed to CSE displayed a marked downregulation of E-cadherin, a transmembrane protein implicated in epithelial cellular adhesion, and a significant upregulation of vimentin and $\alpha$-SMA, which are characteristic markers of fibrogenic and mesenchymal cells, confirming EMT profibrotic remodeling induction by CSE. Interestingly, we observed similar EMT-related alterations in the lung adenocarcinoma cell line, supporting CS role as a driving force of lung cancer progression and metastasis.[46] TGF-$\beta$ is widely recognized as a central mediator of EMT and fibrotic remodeling, promoting fibroblast activation, extracellular matrix deposition, and epithelial plasticity.[47] We further demonstrated that CSE exposure significantly increased TGF-$\beta$ mRNA expression levels in both models, supporting the

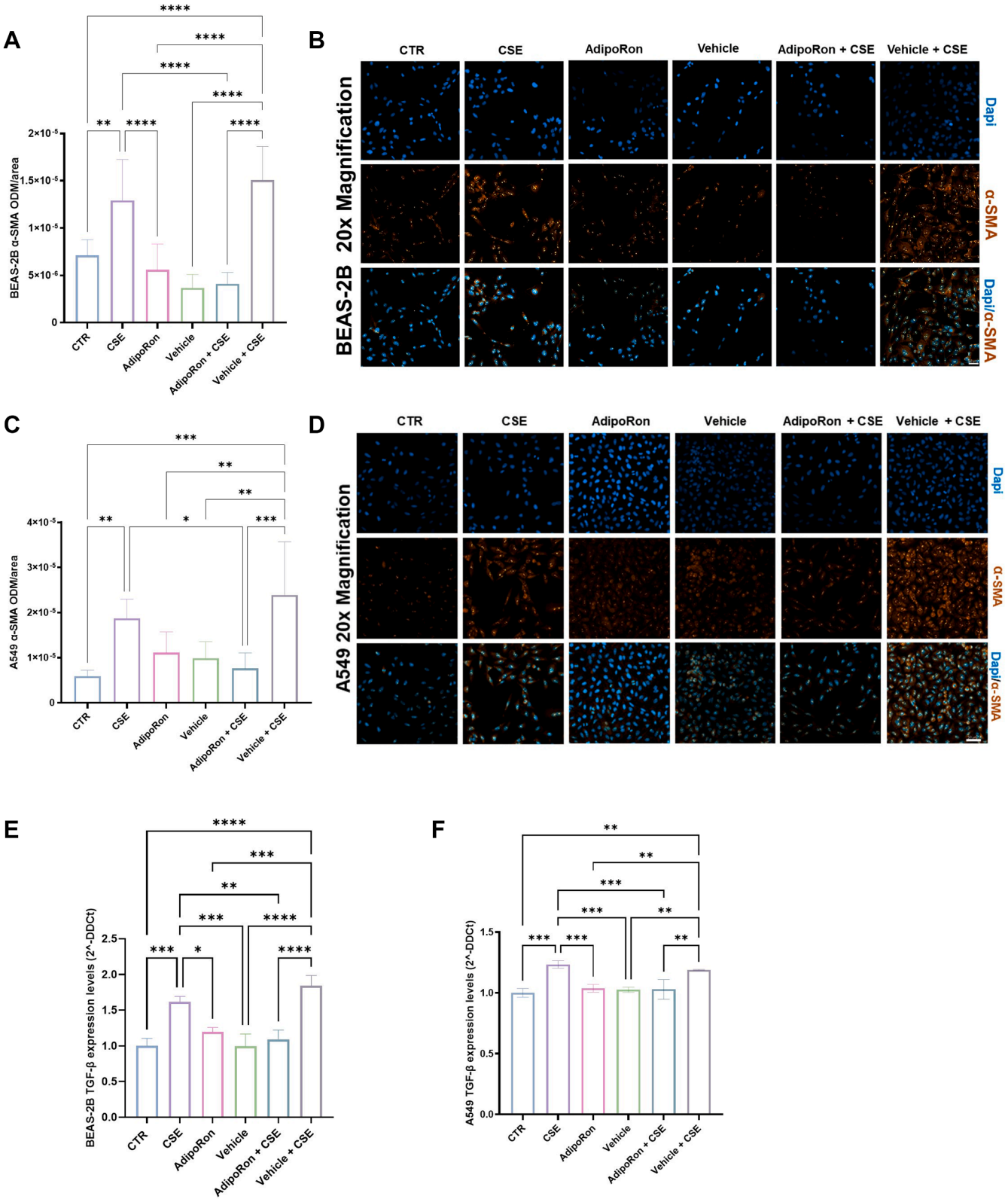


**Fig. 6.** BEAS-2B and A549 cells were used to further explore AR potential in counteracting CSE-induced effects on the expression of the profibrotic mediators $\alpha$-SMA (A and C) and TGF-$\beta$ (E and F) through immunofluorescence staining and RT-PCR, respectively. Cells were pretreated or not for 2 hours with AR and then exposed to CSE for 24 hours before performing immunofluorescence staining and RT-PCR. Data are representative of 3 independent experiments, and values are expressed as mean ± SD. The statistical test used in these analyses was one-way ANOVA followed by Tukey multiple comparison test. *$P < .05$, **$P < .01$, ***$P < .001$, ****$P < .0001$. Representative images of labeled $\alpha$-SMA in BEAS-2B (B) and A549 (D) cells. Scale bar, 50 $\mu$m. Cell fluorescence images were acquired by the Apotome.2 microscope (Zeiss) and analyzed with ImageJ software (NIH).

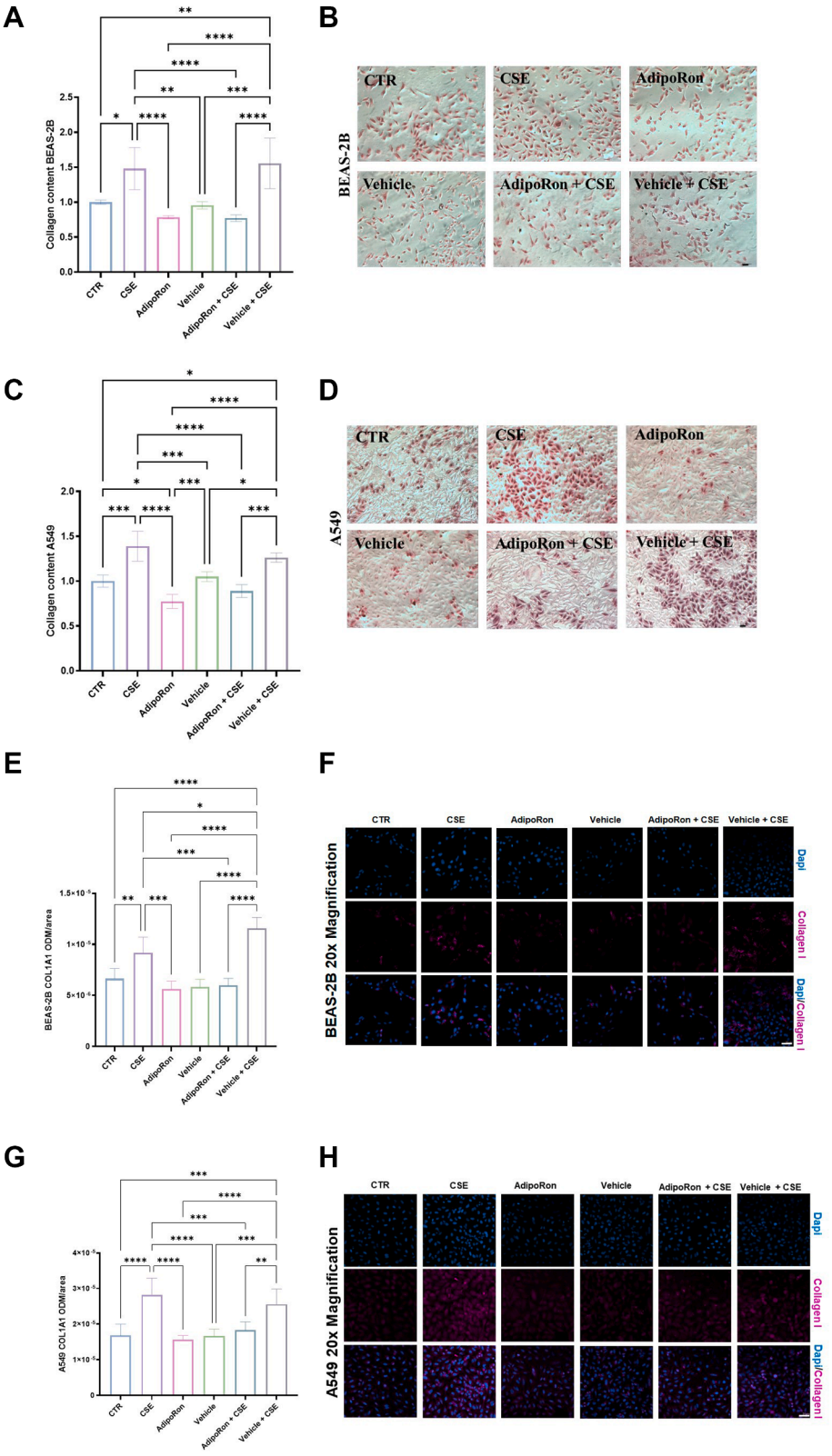


**Fig. 7.** To investigate AR and CSE effects on profibrotic pathways, the expression of total collagen deposition (A and C) and collagen type I protein (E and G) was evaluated in both cell lines through Sirius Red staining and immunofluorescence staining, respectively. Cells were pretreated or not for 2 hours with AR and then exposed to CSE for 24 hours before performing Sirius Red staining and immunofluorescence staining. Data are representative of 3 independent experiments, and values are expressed as mean ± SD. The statistical test used in these analyses was one-way ANOVA followed by Tukey multiple comparison test. *$P < .05$, **$P < .01$, ***$P < .001$, ****$P < .0001$. Representative images of labeled total collagen in BEAS-2B (B) and A549 (D) cells. Scale bar, 100 $\mu$m. Representative images of labeled COL1A1 in BEAS-2B (F) and A549 (H) cells. Scale bar, 50 $\mu$m. Cell fluorescence images were acquired by the Apotome.2 microscope (Zeiss) and analyzed with ImageJ software (NIH).

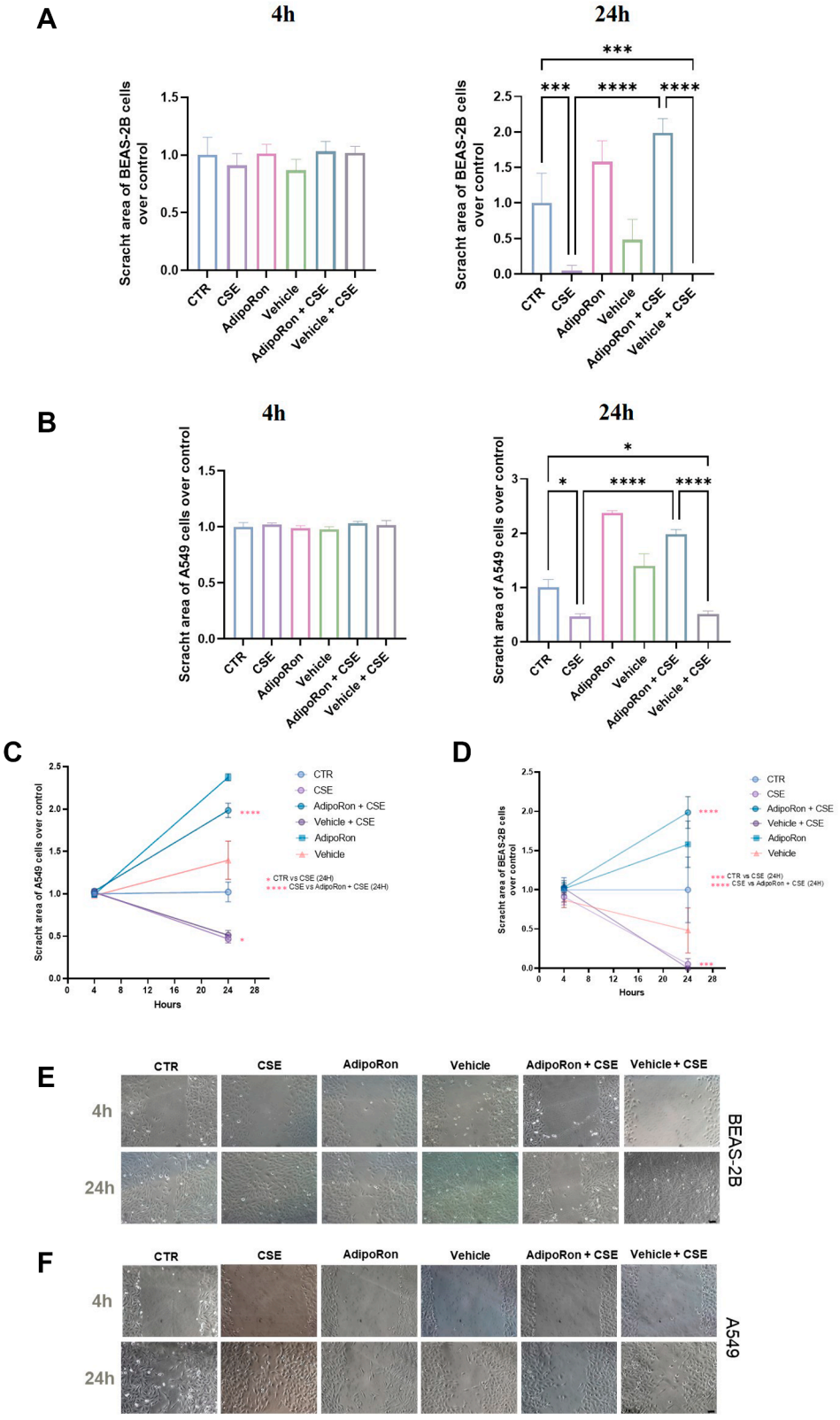


**Fig. 8.** BEAS-2B and A549 cells were used to further explore AR potential in counteracting CSE-induced effects on cell migration through the wound-healing assay. The monolayer was scratched using a tip and washed with PBS to remove detached cells. Then the cells were pretreated or not for 2 hours with AR and then exposed to CSE for 24 hours. The relative closure area of the wound at the chosen time points was normalized to the initial wound area of untreated BEAS-2B (A) and A549 cells (B). Scratch-wound closure over time of BEAS-2B (C) and A549 (D). Representative images of BEAS-2B (E) and A549 (F) scratch profiles in all groups at 4 and 24 hours. Scale bar, 100 $\mu$m. Data are representative of 3 independent experiments, and values are expressed as mean ± SD. The statistical test used in these analyses was one-way ANOVA followed by Tukey multiple comparison test. *$P < .05$, **$P < .01$, ***$P < .001$, ****$P < .0001$.

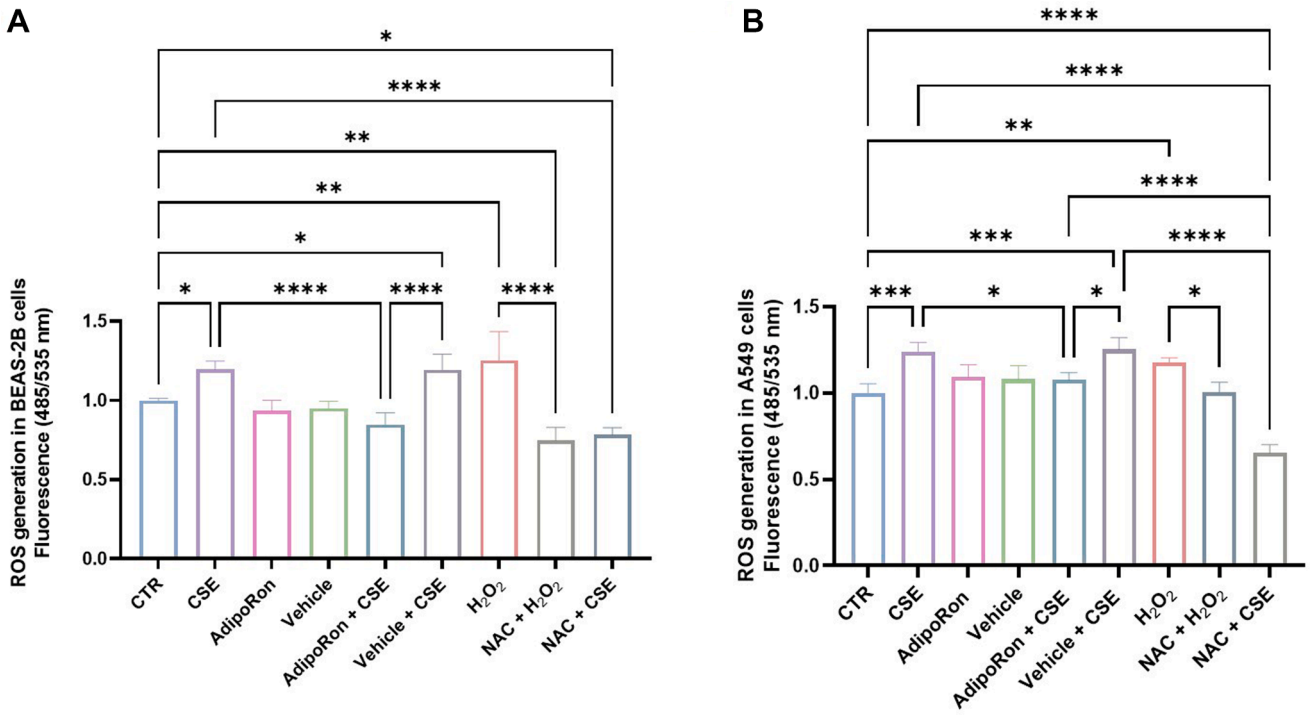


**Fig. 9.** BEAS-2B (A) and A549 cells (B) were used to assess AR and CSE effects on redox balance. The cells were pretreated or not for 2 hours with AR 10 $\mu$g/mL and then exposed to 2% or 10% CSE for 24 hours. Following treatments, ROS generation was determined by the 2′,7′-dichlorodihydrofluorescein diacetate fluorometric assay. The relative ROS production was normalized to the fluorescence intensity of untreated cells. Data are representative of 3 independent experiments, and values are expressed as mean ± SD. The statistical test used in these analyses was one-way ANOVA followed by Tukey multiple comparison test. *$P < .05$, **$P < .01$, ***$P < .001$, ****$P < .0001$.

activation of signaling pathways involved not only in EMT progression but also in fibrotic remodeling. Importantly, the activation of these profibrotic pathways was accompanied by a significant increase in total collagen and COL1A1, indicating that CSE-induced EMT is associated not only with phenotypic epithelial plasticity but also with the establishment of a fibrotic microenvironment. AdipoRon pretreatment effectively mitigated these CSE-induced changes, reducing TGF-$\beta$ expression, preserving the epithelial phenotype, attenuating the mesenchymal shift, and limiting collagen accumulation, suggesting that its protective activity extends beyond EMT modulation and includes the suppression of downstream fibrotic remodeling. Different authors reported that AdipoRon suppresses pro-EMT transcription factors, restoring E-cadherin and vimentin expression levels and attenuating EMT and fibrotic remodeling.[48–51] It has been documented that AdipoR1 knockdown in breast cancer cells leads to enhanced invasion and EMT, suggesting that AdipoR1 and consequently Acrp30 could exert an inhibitory role on EMT and invasive processes.[52] Consistently, previous studies have shown that AdipoRon suppresses both phosphorylated and total nuclear factor $\kappa$B, a key driver of mesenchymal switch, and EMT-related transcription factors counteracting phenotypic transition and cell invasion processes.[53] Furthermore, Li et al[54] demonstrated that AdipoRon alleviates hypertension-induced EMT and renal fibrosis, thereby supporting it as a broad EMT inhibitor across different epithelial models.

### 4.2. Acrp30 prevents CS-induced cell migration and invasive phenotype

Cell migration is a fundamental process involved in physiological as well as pathological conditions, including immune responses, tissue regeneration, and tumor progression. Evaluating cell migration is a crucial functional marker of a mesenchymal phenotype, especially in the context of EMT. Indeed, during EMT epithelial cells lose their intercellular contact, and acquire increased motility and invasiveness.[55] In our models, exposure to CSE was found to enhance the migratory capacity of both normal human bronchial epithelial cells and lung adenocarcinoma cells, providing functional evidence of CS ability to promote a mesenchymal-like phenotype characterized by increased invasive potential. These findings are consistent with previous studies where CS derived, via redox-dependent modifications, the transition toward a mesenchymal phenotype with enhanced migratory capacity.[46,56] Similarly, CS exposure has been reported to promote anchorage-independent growth, as well as migration, invasion, and morphological alterations in mammary epithelial and breast cancer cells.[57] Interestingly, in our study, AdipoRon pretreatment reduced the cells' migratory potential and induced a slower wound healing process in both normal and cancerous cell lines. In agreement with our results, literature data showed Acrp30 ability to suppress proliferation, migration, invasion, and colony formation in thyroid cancer cells, NSCLC cells, and in healthy human colorectal cell lines, highlighting its broad impact on tumor cell behavior.[35,58–60]

### 4.3. Acrp30 protects against CS-induced effects by mitigating oxidative stress

It is fundamental to consider that ROS play an important role as intracellular signaling molecules involved in various pathological conditions, including EMT activation.[61,62] Chronic exposure to CS perpetuates oxidative damage and inflammatory responses in pulmonary tissues, resulting in ongoing tissue injury and aberrant repair processes that contribute to airway structural changes.[31,63–65] In line with this evidence, our data showed that

CSE altered the redox balance of normal BEAS-2B and adenocarcinoma A549 cells, leading to a significant increase in ROS levels. The oxidative stress induced by CSE may thus account, at least in part, for the EMT-related alterations observed in our models. This aligns with previous reports documenting that CSE-induced EMT has been associated with oxidative stress-mediated mechanisms. CSE exposure leads to excessive production of ROS, either directly from smoke components or indirectly through activation of intracellular oxidant-generating systems such as NADPH oxidases.[66] It has been demonstrated that a redox imbalance can trigger redox-sensitive transcriptional reprogramming characteristic of EMT, ultimately leading to alteration in E-cadherin and vimentin markers expression.[61,67] Importantly, we documented that AdipoRon pretreatment confers a protective effect against CSE-induced oxidative stress, attenuating ROS accumulation. Notably, the comparable antioxidant effects observed with NAC and AdipoRon further support the hypothesis that the protective action of AR is, at least in part, mediated through attenuation of ROS-dependent signaling pathways. AdipoRon capacity to mitigate oxidative damage is probably linked to its ability to regulate antioxidant enzymes activity through Acrp30 receptor activation. Indeed, different studies showed that Acrp30 stimulates the increase of superoxide dismutase, catalase, and glutathione peroxidase activity,[68–70] thereby preserving redox homeostasis and preventing ROS-dependent EMT induction.[48–50] As documented in literature by Park et al,[71] overexpression of AdipoR2 reduces oxidative stress by increasing peroxisome proliferator-activated receptor-$\alpha$ activity and catalase expression, exerting protective effects against inflammation and fibrotic progression. This mechanism could explain the observed preservation of epithelial integrity following AdipoRon pretreatment, highlighting Acrp30 potential as a regulator of oxidative stress-mediated epithelial plasticity.

### 4.4. Conclusions

Collectively, these findings highlighted the protective role of AR in counteracting CS-induced EMT onset and fibrosis, by mitigating oxidative stress, preserving epithelial-mesenchymal balance, and reducing migratory capacity in healthy epithelium as well as in tumor progression. One limitation of this study is the lack of investigation into additional molecular mechanisms and the relative contribution of each receptor by which AR could inhibit CS-induced EMT and fibrosis. Nevertheless, these results suggest that AR may offer promising therapeutic potential in preventing airway remodeling and disease progression in smoking-related conditions.

## Abbreviations

Acrp30, adiponectin; AdipoR1, adiponectin receptor 1; AR, AdipoRon; ATCC, American Type Culture Collection; COL1A1, collagen type I $\alpha$1 chain; COPD, chronic obstructive pulmonary disease; CS, cigarette smoke; CSE, cigarette smoke extract; EMT, epithelial-mesenchymal transition; NAC, N-acetylcysteine; NSCLC, non–small cell lung carcinoma; ROS, reactive oxygen species; RT-PCR, reverse transcription polymerase chain reaction; $\alpha$-SMA, $\alpha$-smooth muscle actin; TGF-$\beta$, transforming growth factor-$\beta$.

## Financial support

This research did not receive any specific grant from funding agencies in the public, commercial, or not-for-profit sectors.

## Conflict of interest

The authors declare no conflicts of interest.

## Data availability

The datasets used and/or analyzed during the current study are available from the corresponding author on reasonable request.

## CrediT author contribution statement

**Francesca Panico**: Conceptualization, Data curation, Formal analysis, Investigation, Methodology, Writing – Original draft. **Giuseppe Spaziano**: Conceptualization, Formal analysis, Investigation, Methodology, Writing – Original draft. **Ersilia Nigro**: Data curation, Formal analysis, Investigation, Methodology, Validation. **Davida Mirra**: Conceptualization, Data curation, Project administration, Software, Supervision, Validation, Writing – Review and Editing. **Renata Esposito**: Data curation, Formal analysis, Investigation, Validation, Visualization. **Eleonora Caiazzo**: Formal analysis, Investigation. **Aurora Daniele**: Supervision, Validation, Writing – Review and Editing. **Bruno D'Agostino**: Conceptualization, Funding acquisition, Supervision, Validation, Writing – Review and Editing.

## Supplemental material

This article has supplemental material available at jpet.aspetjournals.org.

## References

1. Nyunoya T, Mebratu Y, Contreras A, Delgado M, Chand HS, Tesfaigzi Y. Molecular processes that drive cigarette smoke-induced epithelial cell fate of the lung. *Am J Respir Cell Mol Biol*. 2014;50(3):471–482. https://doi.org/10.1165/rcmb.2013-0348TR
2. Cappetta D, De Angelis A, Spaziano G, et al. Lung mesenchymal stem cells ameliorate elastase-induced damage in an animal model of emphysema. *Stem Cells Int*. 2018;2018(1):9492038. https://doi.org/10.1155/2018/9492038
3. Padinharayil H, Varghese J, John MC, et al. Non-small cell lung carcinoma (NSCLC): implications on molecular pathology and advances in early diagnostics and therapeutics. *Genes Dis*. 2022;10(3):960–989. https://doi.org/10.1016/j.gendis.2022.07.023
4. Mirra D, Esposito R, Spaziano G, et al. Lung microRNAs expression in lung cancer and COPD: a preliminary study. *Biomedicines*. 2023;11(3):736. https://doi.org/10.3390/biomedicines11030736
5. Steiling K, van den Berge M, Hijazi K, et al. A dynamic bronchial airway gene expression signature of chronic obstructive pulmonary disease and lung function impairment. *Am J Respir Crit Care Med*. 2013;187(9):933–942. https://doi.org/10.1164/rccm.201208-1449OC
6. Tilley AE, Harvey BG, Heguy A, et al. Down-regulation of the notch pathway in human airway epithelium in association with smoking and chronic obstructive pulmonary disease. *Am J Respir Crit Care Med*. 2009;179(6):457–466. https://doi.org/10.1164/rccm.200705-795OC
7. Mirra D, Esposito R, Spaziano G, et al. MicroRNA monitoring in human alveolar macrophages from patients with smoking-related lung diseases: a preliminary study. *Biomedicines*. 2024;12(5):1050. https://doi.org/10.3390/biomedicines12051050
8. Spira A, Beane J, Shah V, et al. Effects of cigarette smoke on the human airway epithelial cell transcriptome. *Proc Natl Acad Sci USA*. 2004;101(27):10143–10148. https://doi.org/10.1073/pnas.0401422101
9. Mirra D, Esposito R, Spaziano G, et al. miRNA signatures in alveolar macrophages related to cigarette smoke: assessment and bioinformatics analysis. *Int J Mol Sci*. 2025;26(3):1277. https://doi.org/10.3390/ijms26031277
10. Gallelli L, D'Agostino B, Marrocco G, et al. Role of tachykinins in the bronchoconstriction induced by HCl intraesophageal instillation in the rabbit. *Life Sci*. 2003;72(10):1135–1142. https://doi.org/10.1016/s0024-3205(02)02372-x
11. Schaible AM, Filosa R, Temml V, et al. Elucidation of the molecular mechanism and the efficacy in vivo of a novel 1,4-benzoquinone that inhibits 5-lipoxygenase. *Br J Pharmacol*. 2014;171(9):2399–2412. https://doi.org/10.1111/bph.12592
12. Yang J, Yan H. Mucosal epithelial cells: the initial sentinels and responders controlling and regulating immune responses to viral infections. *Cell Mol Immunol*. 2021;18(7):1628–1630. https://doi.org/10.1038/s41423-021-00650-7

13. Aoshiba K, Nagai A. Oxidative stress, cell death, and other damage to alveolar epithelial cells induced by cigarette smoke. *Tob Induc Dis*. 2003;1(3):219–226. https://doi.org/10.1186/1617-9625-1-3-219
14. Esposito R, Mirra D, Spaziano G, Panico F, Gallelli L, D'Agostino B. The role of MMPs in the era of CFTR modulators: an additional target for cystic fibrosis patients? *Biomolecules*. 2023;13(2):350. https://doi.org/10.3390/biom13020350
15. Rouget C, Cui YY, D'Agostino B, et al. Nociceptin inhibits airway microvascular leakage induced by HCl intra-oesophageal instillation. *Br J Pharmacol*. 2004;141(6):1077–1083. https://doi.org/10.1038/sj.bjp.0705704
16. D'Agostino B, Advenier C, de Palma R, et al. The involvement of sensory neuropeptides in airway hyper-responsiveness in rabbits sensitized and challenged to *Parietaria judaica*. *Clin Exp Allergy*. 2002;32(3):472–479. https://doi.org/10.1046/j.1365-2222.2002.01328.x
17. Minervini F, Lampridis S, Kestenholz P, et al. The impact of smoking on lung cancer patients. *Eur Respir Rev*. 2025;34(176):240175. https://doi.org/10.1183/16000617.0175-2024
18. Hoffmann RF, Zarrintan S, Brandenburg SM, et al. Prolonged cigarette smoke exposure alters mitochondrial structure and function in airway epithelial cells. *Respir Res*. 2013;14(1):97. https://doi.org/10.1186/1465-9921-14-97
19. Heijink IH, Brandenburg SM, Postma DS, van Oosterhout AJ. Cigarette smoke impairs airway epithelial barrier function and cell-cell contact recovery. *Eur Respir J*. 2012;39(2):419–428. https://doi.org/10.1183/09031936.00193810
20. Alqithami SM, Machwe A, Orren DK. Cigarette smoke-induced epithelial-to-mesenchymal transition: insights into cellular mechanisms and signaling pathways. *Cells*. 2024;13(17):1453. https://doi.org/10.3390/cells13171453
21. Dongre A, Weinberg RA. New insights into the mechanisms of epithelial-mesenchymal transition and implications for cancer. *Nat Rev Mol Cell Biol*. 2019;20(2):69–84. https://doi.org/10.1038/s41580-018-0080-4
22. Xiao D, He J. Epithelial mesenchymal transition and lung cancer. *J Thorac Dis*. 2010;2(3):154–159. https://doi.org/10.3978/j.issn.2072-1439.2010.02.03.7
23. Riemma MA, Cerqua I, Romano B, et al. Sphingosine-1-phosphate/TGF-β axis drives epithelial mesenchymal transition in asthma-like disease. *Br J Pharmacol*. 2022;179(8):1753–1768. https://doi.org/10.1111/bph.15754
24. Popper HH. Progression and metastasis of lung cancer. *Cancer Metastasis Rev*. 2016;35(1):75–91. https://doi.org/10.1007/s10555-016-9618-0
25. Cho ES, Kang HE, Kim NH, Yook JI. Therapeutic implications of cancer epithelial-mesenchymal transition (EMT). *Arch Pharm Res*. 2019;42(1):14–24. https://doi.org/10.1007/s12272-018-01108-7
26. Lu W, Eapen MS, Hardikar A, et al. Epithelial-mesenchymal transition changes in nonsmall cell lung cancer patients with early COPD. *ERJ Open Res*. 2023;9(6):581–2023. https://doi.org/10.1183/23120541.00581-2023
27. Farahzadi R, Valipour B, Fathi E, et al. Oxidative stress regulation and related metabolic pathways in epithelial-mesenchymal transition of breast cancer stem cells. *Stem Cell Res Ther*. 2023;14(1):342. https://doi.org/10.1186/s13287-023-03571-6
28. Morrison D, Rahman I, Lannan S, MacNee WI. Epithelial permeability, inflammation, and oxidant stress in the air spaces of smokers. *Am J Respir Crit Care Med*. 1999;159(2):473–479. https://doi.org/10.1164/ajrccm.159.2.9804080
29. Dhami R, Gilks B, Xie C, Zay K, Wright JL, Churg A. Acute cigarette smoke-induced connective tissue breakdown is mediated by neutrophils and prevented by alpha1-antitrypsin. *Am J Respir Cell Mol Biol*. 2000;22(2):244–252. https://doi.org/10.1165/ajrcmb.22.2.3809
30. Churg A, Zay K, Shay S, et al. Acute cigarette smoke-induced connective tissue breakdown requires both neutrophils and macrophage metalloelastase in mice. *Am J Respir Cell Mol Biol*. 2002;27(3):368–374. https://doi.org/10.1165/rcmb.4791
31. Su X, Wu W, Zhu Z, Lin X, Zeng Y. The effects of epithelial-mesenchymal transitions in COPD induced by cigarette smoke: an update. *Respir Res*. 2022;23(1):225. https://doi.org/10.1186/s12931-022-02153-z
32. Di Zazzo E, Polito R, Bartollino S, et al. Adiponectin as link factor between adipose tissue and cancer. *Int J Mol Sci*. 2019;20(4):839. https://doi.org/10.3390/ijms20040839
33. Summer R, Little FF, Ouchi N, et al. Alveolar macrophage activation and an emphysema-like phenotype in adiponectin-deficient mice. *Am J Physiol Lung Cell Mol Physiol*. 2008;294(6):L1035–L1042. https://doi.org/10.1152/ajplung.00397.2007
34. Nigro E, Perrotta F, Monaco ML, et al. Implications of the adiponectin system in non-small cell lung cancer patients: a case-control study. *Biomolecules*. 2020;10(6):926. https://doi.org/10.3390/biom10060926
35. Cui E, Guo H, Shen M, et al. Adiponectin inhibits migration and invasion by reversing epithelial-mesenchymal transition in non-small cell lung carcinoma. *Oncol Rep*. 2018;40(3):1330–1338. https://doi.org/10.3892/or.2018.6523
36. Bocian-Jastrzębska A, Malczewska-Herman A, Kos-Kudła B. Role of leptin and adiponectin in carcinogenesis. *Cancers*. 2023;15(17):4250. https://doi.org/10.3390/cancers15174250
37. Kotani K, Hazama A, Hagimoto A, et al. Adiponectin and smoking status: a systematic review. *J Atheroscler Thromb*. 2012;19(9):787–794. https://doi.org/10.5551/jat.11833
38. Gu D, Shi Y, Gong Z, et al. AdipoRon, an adiponectin receptor agonist, protects contrast-induced nephropathy by suppressing oxidative stress and inflammation via activation of the AMPK pathway. *Clin Exp Nephrol*. 2020;24(11):989–998. https://doi.org/10.1007/s10157-020-01944-2
39. Panico F, Mirra D, Petito G, et al. Protective action of 3,5-diiodo-L-thyronine on cigarette smoke-induced mitochondrial dysfunction in human alveolar epithelial cells. *Biomedicines*. 2025;13(5):1014. https://doi.org/10.3390/biomedicines13051014
40. Zhang YZ, Zhang YL, Huang Q, et al. AdipoRon alleviates free fatty acid-induced myocardial cell injury via suppressing Nlrp3 inflammasome activation. *Diabetes Metab Syndr Obes*. 2019;12:2165–2179. https://doi.org/10.2147/DMSO.S221841
41. Yao R, Cao Y, He YR, Lau WB, Zeng Z, Liang ZA. Adiponectin attenuates lung fibroblasts activation and pulmonary fibrosis induced by paraquat. *PLoS One*. 2015;10(5):e0125169. https://doi.org/10.1371/journal.pone.0125169
42. Wang Y, Wan Y, Ye G, et al. Hepatoprotective effects of AdipoRon against d-galactosamine-induced liver injury in mice. *Eur J Pharm Sci*. 2016;93:123–131. https://doi.org/10.1016/j.ejps.2016.08.017
43. Davigo M, Van Schooten FJ, Wijnhoven B, et al. Alterations in the molecular regulation of mitochondrial metabolism in human alveolar epithelial cells in response to cigarette- and heated tobacco product emissions. *Toxicol Lett*. 2024;401:89–100. https://doi.org/10.1016/j.toxlet.2024.09.004
44. Xu L, Li X, Wang H, Xie F, Liu H, Xie J. Cigarette smoke triggers inflammation mediated by autophagy in BEAS-2B cells. *Ecotoxicol Environ Saf*. 2019;184:109617. https://doi.org/10.1016/j.ecoenv.2019.109617
45. Sohal SS, Reid D, Soltani A, et al. Reticular basement membrane fragmentation and potential epithelial mesenchymal transition is exaggerated in the airways of smokers with chronic obstructive pulmonary disease. *Respirology*. 2010;15(6):930–938. https://doi.org/10.1111/j.1440-1843.2010.01808.x
46. Sharma JR, Agraval H, Yadav UCS. Cigarette smoke induces epithelial-to-mesenchymal transition, stemness, and metastasis in lung adenocarcinoma cells via upregulated RUNX-2/galectin-3 pathway. *Life Sci*. 2023;318:121480. https://doi.org/10.1016/j.lfs.2023.121480
47. Lee JH, Massagué J. TGF-$\beta$ in developmental and fibrogenic EMTs. *Semin Cancer Biol*. 2022;86:136–145. https://doi.org/10.1016/j.semcancer.2022.09.004
48. Kim AY, Lee YS, Kim KH, et al. Adiponectin represses colon cancer cell proliferation via AdipoR1- and -R2-mediated AMPK activation. *Mol Endocrinol*. 2010;24(7):1441–1452. https://doi.org/10.1210/me.2009-0498
49. Liang M, Li JW, Luo H, et al. Epithelial-mesenchymal transition suppresses AMPK and sensitizes cancer cells to pyroptosis under energy stress. *Cells*. 2022;11(14):2208. https://doi.org/10.3390/cells11142208
50. Zhang Z, Du J, Xu Q, et al. Adiponectin suppresses metastasis of nasopharyngeal carcinoma through blocking the activation of NF-κB and STAT3 signaling. *Int J Mol Sci*. 2022;23(21):12729. https://doi.org/10.3390/ijms232112729
51. Wang X, Yang J, Wu L, et al. Adiponectin inhibits the activation of lung fibroblasts and pulmonary fibrosis by regulating the nuclear factor kappa B (NF-κB) pathway. *Bioengineered*. 2022;13(4):10098–10110. https://doi.org/10.1080/21655979.2022.2063652
52. Hwang MS, Yu N, Stinson SY, et al. miR-221/222 targets adiponectin receptor 1 to promote the epithelial-to-mesenchymal transition in breast cancer. *PLoS One*. 2013;8(6):e66502. https://doi.org/10.1371/journal.pone.0066502
53. Kashiwagi E, Abe T, Kinoshita F, et al. The role of adipocytokines and their receptors in bladder cancer: expression of adiponectin or leptin is an independent prognosticator. *Am J Transl Res*. 2020;12(6):3033–3045.
54. Li Y, Song B, Ruan C, Xue W, Zhao J. AdipoRon attenuates hypertension-induced epithelial-mesenchymal transition and renal fibrosis via promoting epithelial autophagy. *J Cardiovasc Transl Res*. 2021;14(3):538–545. https://doi.org/10.1007/s12265-020-10075-8
55. Gandalovičová A, Vomastek T, Rosel D, Brábek J. Cell polarity signaling in the plasticity of cancer cell invasiveness. *Oncotarget*. 2016;7(18):25022–25049. https://doi.org/10.18632/oncotarget.7214
56. Zhang H, Liu H, Borok Z, Davies KJA, Ursini F, Forman HJ. Cigarette smoke extract stimulates epithelial-mesenchymal transition through Src activation. *Free Radic Biol Med*. 2012;52(8):1437–1442. https://doi.org/10.1016/j.freeradbiomed.2012.01.024
57. Di Cello F, Flowers VL, Li H, et al. Cigarette smoke induces epithelial to mesenchymal transition and increases the metastatic ability of breast cancer cells. *Mol Cancer*. 2013;12(1):90. https://doi.org/10.1186/1476-4598-12-90
58. Li C, Zhang J, Dionigi G, Liang N, Guan H, Sun H. Uncovering the connection between obesity and thyroid cancer: the therapeutic potential of adiponectin receptor agonist in the AdipoR2-ULK axis. *Cell Death Dis*. 2024;15(9):708. https://doi.org/10.1038/s41419-024-07084-9
59. Nigro E, Stiuso P, Matera MG, et al. The anti-proliferative effects of adiponectin on human lung adenocarcinoma A549 cells and oxidative stress involvement. *Pulm Pharmacol Ther*. 2019;55:25–30. https://doi.org/10.1016/j.pupt.2019.01.004
60. Nigro E, Schettino P, Polito R, et al. Adiponectin and colon cancer: evidence for inhibitory effects on viability and migration of human colorectal cell lines. *Mol Cell Biochem*. 2018;448(1–2):125–135. https://doi.org/10.1007/s11010-018-3319-7
61. Lee SY, Ju MK, Jeon HM, et al. Reactive oxygen species induce epithelial-mesenchymal transition, glycolytic switch, and mitochondrial repression through the Dlx-2/Snail signaling pathways in MCF-7 cells. *Mol Med Rep*. 2019;20(3):2339–2346. https://doi.org/10.3892/mmr.2019.10466
62. Aggarwal V, Tuli HS, Varol A, et al. Role of reactive oxygen species in cancer progression: molecular mechanisms and recent advancements. *Biomolecules*. 2019;9(11):735. https://doi.org/10.3390/biom9110735
63. Seagrave J. Oxidative mechanisms in tobacco smoke-induced emphysema. *J Toxicol Environ Health A*. 2000;61(1):69–78. https://doi.org/10.1080/00984100050116799

64. Seo YS, Park JM, Kim JH, Lee MY. Cigarette smoke-induced reactive oxygen species formation: a concise review. *Antioxidants (Basel)*. 2023;12(9):1732. https://doi.org/10.3390/antiox12091732, 2023.
65. Padmavathi P, Raghu PS, Reddy VD, et al. Chronic cigarette smoking-induced oxidative/nitrosative stress in human erythrocytes and platelets. *Mol Cell Toxicol*. 2018;14(1):27–34. https://doi.org/10.1007/s13273-018-0004-6
66. Milara J, Peiró T, Serrano A, Cortijo J. Epithelial to mesenchymal transition is increased in patients with COPD and induced by cigarette smoke. *Thorax*. 2013;68(5):410–420. https://doi.org/10.1136/thoraxjnl-2012-201761
67. Jiang J, Wang K, Chen Y, Chen H, Nice EC, Huang C. Redox regulation in tumor cell epithelial-mesenchymal transition: molecular basis and therapeutic strategy. *Signal Trans Target Ther*. 2017;2(1):17036. https://doi.org/10.1038/sigtrans.2017.36
68. Liu Y, Palanivel R, Rai E, et al. Adiponectin stimulates autophagy and reduces oxidative stress to enhance insulin sensitivity during high-fat diet feeding in mice. *Diabetes*. 2015;64(1):36–48. https://doi.org/10.2337/db14-0267
69. Lu JP, Hou ZF, Duivenvoorden WC, Whelan K, Honig A, Pinthus JH. Adiponectin inhibits oxidative stress in human prostate carcinoma cells. *Prostate Cancer Prostatic Dis*. 2012;15(1):28–35. https://doi.org/10.1038/pcan.2011.53
70. Tilija Pun N, Park PH. Role of p62 in the suppression of inflammatory cytokine production by adiponectin in macrophages: involvement of autophagy and p21/Nrf2 axis. *Sci Rep*. 2017;7(1):393. https://doi.org/10.1038/s41598-017-00456-6
71. Park PH, Sanz-Garcia C, Nagy LE. Adiponectin as an anti-fibrotic and anti-inflammatory adipokine in the liver. *Curr Pathobiol Rep*. 2015;3(4):243–252. https://doi.org/10.1007/s40139-015-0094-y